Geophysical Research Letters

RESEARCH LETTER
10.1029/2019GL082903

Daytime Evolution of Equatorial Plasma Bubbles Observed by the First Republic of China Satellite

Hyosub Kil[1], Larry J. Paxton[1], Woo Kyoung Lee[2,3], and Geonhwa Jee[4]

[1]Applied Physics Laboratory, The Johns Hopkins University, Laurel, MD, USA, [2]Korea Astronomy and Space Science Institute, Daejeon, Republic of Korea, [3]University of Science and Technology, Daejeon, Republic of Korea, [4]Korea Polar Research Institute, Incheon, Republic of Korea

Key Points:
- Daytime electron density irregularities in the low latitude *F* region are associated with bubbles developed on previous nights
- The locations of daytime irregularities move from the magnetic equator to higher latitudes as time progresses
- Daytime irregularity distribution is consistent with the daytime ambient plasma motion induced by the ionospheric fountain effect

Correspondence to:
H. Kil,
hyosub.kil@jhuapl.edu

Citation:
Kil, H., Paxton, L. J., Lee, W. K., & Jee, G. (2019). Daytime evolution of equatorial plasma bubbles observed by the first Republic of China satellite. *Geophysical Research Letters*, *46*, 5021–5027. https://doi.org/10.1029/2019GL082903

Received 19 MAR 2019
Accepted 1 MAY 2019
Accepted article online 6 MAY 2019
Published online 22 MAY 2019

Abstract Plasma bubbles in the equatorial *F* region are thought of as nighttime phenomena because they develop at night and are assumed to vanish after sunrise. However, bubbles occasionally persist throughout the night and into the day. This study investigates the origin of daytime irregularities and their evolution using data from the first Republic of China satellite. Our results show that daytime irregularities occur in the longitudes where bubbles have developed on previous nights. A newly reported feature is the observation of the temporal variation of the locations of daytime irregularities; daytime irregularities are concentrated near the magnetic equator early in the morning, but the location gradually shifts to higher latitudes with time. This phenomenon is explained in terms of the latitudinal redistribution of fossil bubbles by the ionospheric fountain effect.

Plain Language Summary Severe electron density disturbances are created at night in the equatorial ionosphere by the upward transport of the low-density plasma from the bottomside of the ionosphere. These phenomena are called bubbles because the plasma density at the locations of the disturbances is smaller than that of the ambient plasma. Bubbles are thought of as nighttime phenomena because bubbles develop after sunset and decay away after sunrise. However, our study using satellite data shows that some parts of these nighttime bubbles survive through the day and become the major sources of daytime electron density irregularities. The new finding of our study is that the locations of daytime irregularities move from the magnetic equator to higher latitudes over time. The redistribution of fossil bubbles is driven by the same ionospheric electrodynamics that creates the ionospheric equatorial arcs.

1. Introduction

Plasma bubbles in the equatorial *F* region consist of plasma depletions with respect to ambient plasma. The plasma depletion in a bubble is related to the formation of a bubble by the transport of low-density plasma from the bottomside of the *F* region to the topside (e.g., Woodman & La Hoz, 1976). Typically, bubbles develop after sunset by the generalized Rayleigh-Taylor instability and disappear after sunrise. However, bubbles also develop late at night under special conditions such as geomagnetic storms or low solar activity (e.g., Heelis et al., 2010; Smith & Heelis, 2018).

Nighttime bubbles have been observed by various techniques. They appear as plasma depletions in in situ measurements (e.g., Burke et al., 2004; Hanson & Sanatani, 1973; Huang et al., 2013; Kil et al., 2009; Kil & Heelis, 1998; Su et al., 2006), spread *F* in ionosonde data (e.g., Abdu et al., 2012; Narayanan et al., 2014), emission depletion bands in optical observations (e.g., Immel et al., 2003; Kil et al., 2004; Makela & Kelley, 2003; Martinis et al., 2003; Mendillo & Baumgardner, 1982; Pimenta et al., 2003; Shiokawa et al., 2004), and vertical plumes in radar backscatter power maps (e.g., Hysell et al., 2005; Kudeki & Bhattacharyya, 1999; Tsunoda, 1983; Yokoyama et al., 2011). However, little is known about daytime bubble signatures. One reason may be that bubble signatures are difficult to detect during daytime. Optical observations are not usable for the detection of daytime bubbles because the airglow during daytime is dominated by Rayleigh scattering of sunlight by the troposphere that is thousands of times brighter than the ionospheric signal. Fossils of nighttime bubbles in the topside are not detectable by ionosondes on the ground. Daytime backscatter echoes have been detected in the upper ionosphere by the radar at Jicamarca (Chau & Woodman, 2001; Woodman et al., 1985), but they are rare events and their connection with bubbles has not yet been verified.

The daytime signatures of bubbles were identified from the measurements of the electron density by the Communication/Navigation Outage Forecasting System satellite. Huang et al. (2013) reported several events of daytime irregularities associated with bubbles on previous nights from the Communication/Navigation Outage Forecasting System observations. This observational result indicated that the lifetime of a bubble is much longer than we usually think of it as being. Huang et al. (2013) attributed the detection of long-lasting bubbles in the upper ionosphere (~800 km) to the low photoionization (or refilling) rate at high altitudes. However, the lifetime of a bubble would also be affected by other factors such as the plasma depletion depth, solar zenith angle, and solar activity. We do not yet have an accurate or complete knowledge of the conditions required for bubbles to persist until they can be observed on the dayside.

This study reports on daytime irregularities identified from the first Republic of China satellite (ROCSAT-1) observations. Our investigation focuses on the origin of daytime irregularities and the role of ionospheric dynamics in the evolution of bubbles during daytime. Section 2 describes the ROCSAT-1 data and detection method of daytime irregularities. Observational results are presented in section 3. In section 4, we discuss the factors that affect the evolution of a bubble during daytime. Conclusions are given in section 5.

2. Data Description

ROCSAT-1 (later renamed as Formosat-1) was a low-earth-orbit satellite operated by Taiwan for the purpose of the observations of the Earth's ionosphere and oceans. ROCSAT-1 was launched on 27 January 1999, and the mission ended on 17 June 2004. The satellite was in a near-circular orbit at an altitude of 600 km with an orbital inclination of 35°. The orbital period was 97 min. The Plasma and Electrodynamics Instrument was one of the three payloads on ROCSAT-1, and it measured the ion composition, electron and ion temperatures, and ion velocities. Our study uses the measurements of the total ion density with the data sampling cadence of 1 s.

The ROCSAT-1 observations on 17 November 1999 are shown in Figure 1 to compare nighttime and daytime bubble features. The parameter S in the bottom panel is an indicator of the electron density fluctuation and is defined as

$$S = \left[\frac{1}{n-1}\sum_{i=0}^{n-1}(\log_{10}N_i - L_i)^2\right]^{1/2}.$$

Here N_i is the electron density, L_i is the linear fit of $\log_{10}N_i$ and is used for the detrending of the data, and n is the number of data points. In our study, S is calculated with 10 data points. Bubbles at night are pronounced features, as we can identify by the plasma depletions in the red shaded regions. The irregularities detected after sunrise are indicated by the green shading. Figure 1b shows an enlarged plot of the density in the green shaded region with the parameter S. In previous studies (Kil et al., 2009; Su et al., 2006), standard deviations normalized by the mean density (i.e., S/mean(L_i)) were used for the detection of nighttime irregularities from ROCSAT-1 data. The threshold used for the detection of nighttime bubbles by those previous studies was 0.003, which corresponds to $S = 0.015$ when the logarithm of the mean density is 5. The S values at the locations of nighttime bubbles are well over this threshold, but, as we can see in Figure 1b, the majority of daytime irregularities are not detected by this threshold. The use of S or S/mean(L_i) does not make a significant difference in the irregularity detection.

3. Observational Results

Daytime irregularities show various morphologies. Some irregularities, specially the irregularities detected in the morning sector as shown in Figure 1, maintain the bubble morphology (plasma depletions), but in many cases, daytime irregularities show irregular fluctuations. The examples in Figure 2 observed on 2 October 2001 show the typical morphology of daytime irregularities in the afternoon. Irregularities can be identified at the locations where the S value is greater than the base value (~0.0005). We interpret these irregularities as fossils of bubbles because bubbles were observed to have developed after midnight at the longitudes of those irregularities. Huang et al. (2013) reported bubbles that lasted until 15 hr local time (LT) at an altitude of 800 km. The events in Figure 2 show that bubbles at an altitude of 600 km can also last throughout the afternoon. Note the detection of the irregularities at 10–20° magnetic latitudes and the

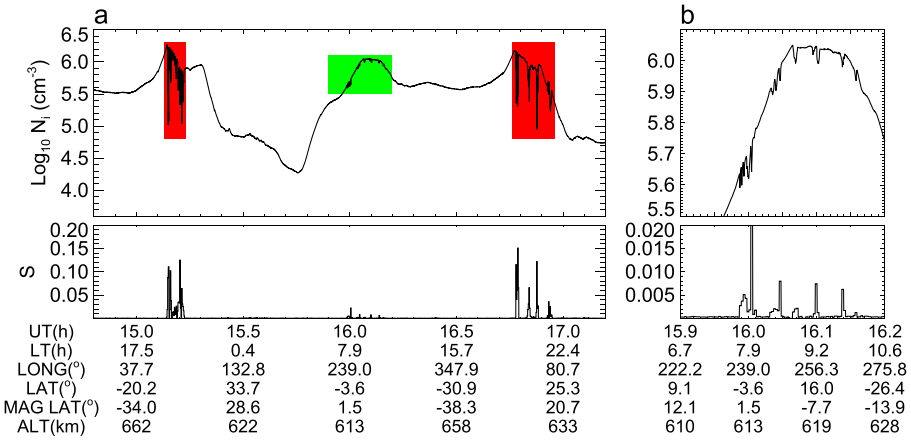

Figure 1. (a) Comparison of nighttime (red shaded area) and daytime (green shaded area) irregularities in the first Republic of China satellite observations on 17 November 1999. *S* represents the standard deviation of the logarithm of the density fluctuation after the detrending of the data. (b) Enlarged data in the green shaded region in Figure 1a.

absence of the irregularities near the magnetic equator. ROCSAT-1 passed the magnetic equator at 0.78 hr universal time (UT; left panel) and 4.04 hr UT (right panel), respectively. The irregularities along the ROCSAT-1 passes occur at different magnetic meridians, and therefore, their occurrence can be understood as longitudinal variation instead of latitudinal variation. However, the occurrence of the irregularities in low latitudes in the absence of their occurrence at the magnetic equator is often observed in ROCSAT-1 data. Later, we discuss this phenomenon using the latitudinal distribution of the irregularities (summarized in Figure 4).

The ROCSAT-1 observations on consecutive orbits enable us to examine the origin of daytime irregularities. We illustrate our method using the ROCSAT-1 observations on (a) 7 April 2000 and (b) 16 April 2004 in Figure 3. On both days, the observations on orbit 1 are provided to show the development of intense bubbles on previous nights at the longitudes where daytime irregularities are detected. The locations of nighttime bubbles and daytime irregularities are indicated in red on the plots of the ground traces of the orbits. The bubbles on orbit 1 maintain deep depletions, although they are detected after midnight. We could not identify whether those bubbles were created before midnight because the ROCSAT-1 orbits before midnight were too far away from the magnetic equator. Regardless of their creation time, the maintenance of deep depletions until sunrise seems to be an important condition for the survival of bubbles after sunrise.

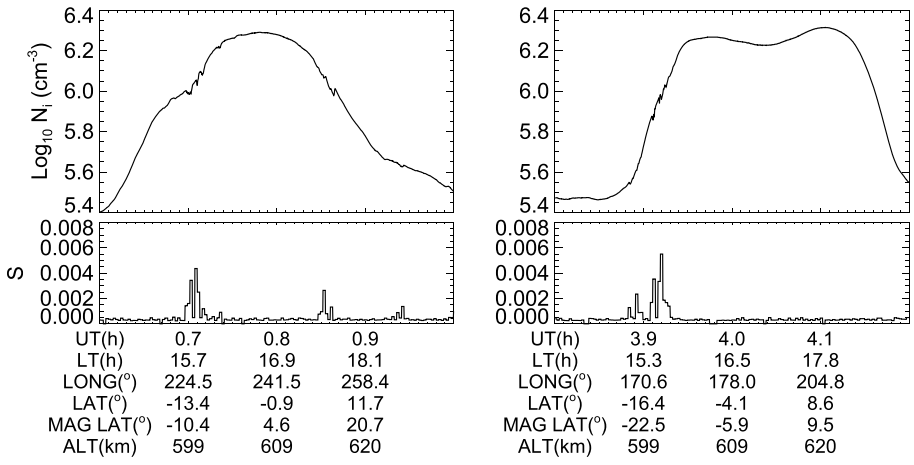

Figure 2. Examples of afternoon irregularities observed on 2 October 2001. Irregularities can be identified at the locations where the *S* value is greater than the base value (~0.0005). Note the absence of the irregularities at the magnetic equator.

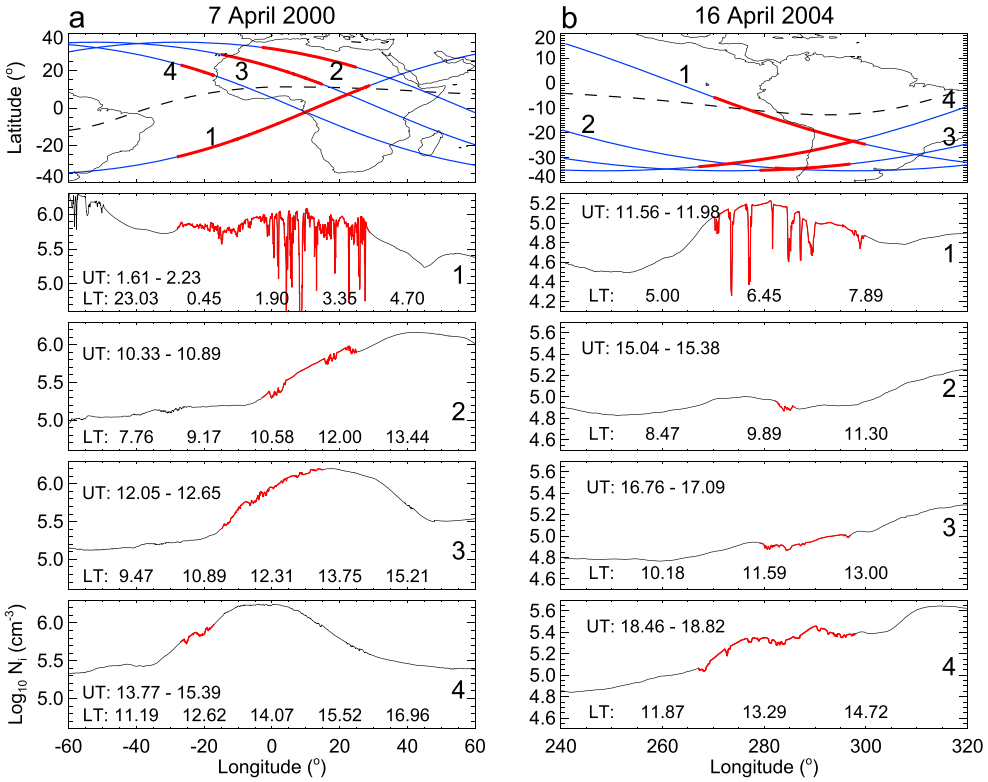

Figure 3. Series of first Republic of China satellite (ROCSAT-1) observations on (a) 7 April 2000 and (b) 16 April 2004. The detection locations of bubbles at night and daytime irregularities are indicated in red on the ROCSAT-1 orbit tracks and density measurements. The black dashed lines in the top panels indicate the magnetic equator.

On orbit 4 in Figure 3a, irregularities appear around 10°N magnetic latitude, but irregularities are not detected at the magnetic equator. This observation is similar to the observations in Figure 2.

We have traced the history of 50 events of daytime irregularities using the method shown in Figure 3. The association of daytime irregularities with bubbles on the previous night was identified for the majority of the daytime irregularity events. We could not determine the association of daytime irregularities with

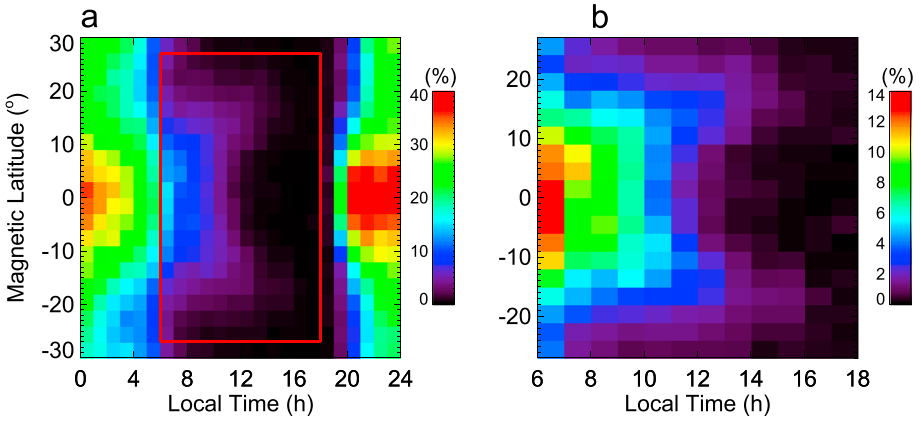

Figure 4. (a) Distribution of the irregularities obtained using the threshold $S > 0.002$. (b) Enlarged image of the red box in Figure 4a. Note the change in the color bar scale of a factor of 3. The distribution is derived using all the first Republic of China satellite data acquired from March 1999 to June 2004. The occurrence probability is determined by the ratio of the number of orbits with irregularities to the total number of orbits.

nighttime bubbles for a few events because ROCSAT-1 orbits were too far away from the magnetic equator to identify the occurrence of bubbles at night. This investigation result indicates that daytime irregularities in low latitudes can be interpreted to be fossils of nighttime bubbles.

From many daytime irregularity events including the events in Figures 1–3, we have noticed the occurrence of daytime irregularities outside of the magnetic equator. To verify this property, the latitudinal distribution of the irregularities is derived using all ROCSAT-1 data acquired from March 1999 to June 2004. Figure 4a shows the occurrence probability of the irregularities as a function of LT and magnetic latitude. The threshold value of S used for the detection of irregularities is 0.002. The S values at the locations of nighttime bubbles are several times greater than this threshold, but only large amplitudes of daytime irregularities are detected with this threshold. To minimize any detection errors of daytime irregularities, we use the threshold that is well over the base value (0.0005) at quiet regions. For each 1-hr and 3° bin, the occurrence probability is determined by the ratio of the number of orbits with irregularities to the total number of orbits. We examine the temporal variation of the occurrence rate from the evening in order to track the evolution of bubbles from the development. The occurrence rate abruptly increases from near zero to 20% at 19 hr LT in the equatorial region. This observation is consistent with our understanding of the development of bubbles just after sunset. The peak of the occurrence rate appears around 22 hr LT. From the figure, we can identify the increasing latitudinal extension of the locations of the irregularities with time during 19–22 hr LT. This phenomenon is expected to be arising from the growth of bubbles during that time period. The retraction of the irregularity locations to the equatorial region after midnight may be explained by the decay of the bubbles and the downward motion of the ionosphere at night. The occurrence rate rapidly decreases after around 6–7 hr LT (or after sunrise) due to the filling of the bubbles by the photoionization of oxygen atoms. However, the decrease of the occurrence rate at the sunrise terminator is not as dramatic as the rapid increase of the occurrence rate at the sunset terminator. The relatively gradual decrease of the occurrence rate at the sunrise terminator may indicate that some portion of the topside signature of nighttime bubbles could survive after sunrise. In Figure 4a, irregularities are not confined to low latitudes at night. Traveling ionospheric disturbances are considered to be important sources of the irregularities beyond low latitudes, but the latitudinal boundary of the irregularities associated with bubbles and traveling ionospheric disturbances is not distinguishable from the observational data.

The occurrence rate of the irregularities during daytime is a few times smaller than that of the irregularities at night. An interesting feature in the distribution of the irregularities during daytime is the temporal variation of the irregularity location. Figure 4b is the enlarged image of the red box in Figure 4a using a different color scale. Irregularities are concentrated within ±10° magnetic latitudes in the morning. The concentration location gradually moves to higher latitudes in both hemispheres as time progresses, and the concentration peak appears around ±15° magnetic latitudes in the afternoon. This phenomenon has not yet been reported. This phenomenon is considered to indicate the involvement of ionospheric dynamics in the evolution of bubbles during daytime.

4. Discussion

Our study and the results in Huang et al. (2013) suggest that nighttime bubbles are important sources of daytime irregularities over low latitudes. The irregularity distribution in Figure 4 further supports this interpretation. The occurrence rate of the irregularities rapidly decreases after sunrise and keeps decreasing with time. This observation may be explained as due to the decay of bubbles. If the daytime irregularities were produced by new sources during daytime (by traveling ionospheric disturbances, for example), the occurrence rate would not show such a continuously decreasing trend with time. As long as daytime irregularities are associated with nighttime bubbles, the occurrence of daytime irregularities is closely related to the lifetime of bubbles. Huang et al. (2013) pointed out that bubbles at higher altitudes can survive longer because the ion/electron production rate decreases with altitudes. The rapid decrease of the occurrence rate of the irregularities after sunrise can be interpreted to be an indication of the significant role of photoionization in the decay of a bubble. However, the lifetime of a bubble during daytime is also a function of its creation local time and the depletion depth during that time. A bubble created after midnight has a higher chance to last till sunrise and beyond than does a bubble created before midnight. A deeper bubble will also have a higher chance to survive as a detectable event during daytime. The other factors that may affect the

lifetime of a bubble are the solar zenith angle and the solar flux. Bubbles will decay or be filled in faster near the equator than far away from the equator and in the summer hemisphere than in the winter hemisphere due to the difference in solar zenith angle. We also expect a longer lifetime for a daytime bubble during solar minimum than during solar maximum due to the difference in the photoionization rate. However, the depletion depth and the solar local time of the creation of a bubble can vary with the solar cycle. Numerical simulations of a bubble under various conditions are desirable to identify the contributions of different factors to the lifetime of a bubble.

The temporal variation of the latitudinal distribution of daytime irregularities is a new phenomenon that has not heretofore been reported. The higher occurrence rate of daytime irregularities outside of the magnetic equator than at the magnetic equator appears to contradict our interpretation that daytime irregularities are fossils of nighttime bubbles. If nighttime bubbles were the sources of daytime irregularities, daytime irregularities would appear in the equatorial region where bubbles had developed at night. The discrepancy between the latitudinal locations of nighttime bubbles and daytime irregularities can be explained in association with the daytime plasma motion. In the equatorial *F* region, plasma experiences a rapid upward motion after sunrise reaching its peak velocity at around 11 hr LT (Fejer et al., 1991; Kil et al., 2009). Then, the upward velocity gradually decreases until the sunset time. The upward motion during daytime accompanies plasma diffusion along magnetic field lines. These processes are known as the ionospheric *fountain effect* (Hanson & Moffett, 1966). The diffusion of equatorial plasma creates the ionization trough at the magnetic equator and the ionization anomaly around ±10°–15° magnetic latitudes. Because fossil bubbles move with the ambient plasma, they are often used as tracers of the motion of the background ionosphere (e.g., Tsunoda et al., 1981). Therefore, fossil bubbles are expected to follow the path of the ambient plasma. In Figure 4, irregularities are concentrated in the equatorial region at night. The separation of the region of peak concentration occurs in the morning and increases with time. This behavior is consistent with the formation of the ionization trough and anomaly during daytime by the fountain effect. The latitudinal expansion of the irregularity location in the afternoon can also be explained by the simple uplift of the bubble-embedded ionosphere without the transport of bubbles along the magnetic field lines. However, the simple uplift mechanism cannot explain the lower occurrence rate of bubbles at the magnetic equator than outside of the magnetic equator. Without the transport of bubbles along the magnetic field lines, bubbles would be detected more frequently at the magnetic equator than anywhere else because, without transport, bubbles would originate from the magnetic equatorial region.

Finally, we note the effect of the fountain effect on the lifetime of a bubble during daytime. The upward motion of the ionosphere transports bubbles to higher altitudes where the ion/electron production rate is smaller. Therefore, the ionospheric vertical motion during daytime acts to increase the lifetime of a bubble. The displacement of equatorial bubbles to higher latitudes slows down their decay because the solar zenith angle increases with latitude. Thus, the background ionospheric dynamics should also be taken into account with other factors described above for a comprehensive understanding of the lifetime of a bubble.

5. Conclusions

The source and evolution of daytime irregularities in the low latitude *F* region are investigated using the in situ measurements of the ion density by ROCSAT-1 satellite. Our results show that daytime irregularities detected at low latitudes can be associated with nighttime bubbles. This conclusion is supported by the observations of bubbles on previous nights in the longitudes where daytime irregularities are detected. A new finding of our study is the temporal variation of the locations of daytime irregularities; irregularities are concentrated at the magnetic equator early in the morning, but the concentration location gradually moves to higher latitudes with time. This phenomenon is consistent with the transport of the ambient plasma driven by the fountain effect. Numerical simulations are necessary to identify the effect of the ionospheric dynamics on the evolution (or distribution) of bubbles and the factors that affect the lifetime of a bubble.

Acknowledgments
The work at JHU/APL was supported by MURI FA9559-16-1-0364 and KOPRI PE18020 awards. W. K. Lee acknowledges the support from the basic research fund from KASI and National Research Foundation of Korea (NRF-2018R1C1B6006700). The ROCSAT-1 data are available the from NASA heliophysics data portal (https://heliophysicsdata.sci.gsfc.nasa.gov/websearch/dispatcher).

References

Abdu, M. A., Batista, I. S., Reinisch, B. W., MacDougall, J. W., Kherani, E. A., & Sobral, J. H. A. (2012). Equatorial range spread *F* echoes from coherent backscatter, and irregularity growth processes, from conjugate point digital ionograms. *Radio Science*, *47*, RS6003. https://doi.org/10.1029/2012RS005002

Burke, W. J., Gentile, L. C., Huang, C. Y., Valladares, C. E., & Su, S.-Y. (2004). Longitudinal variability of equatorial plasma bubbles observed by DMSP and ROCSAT-1. *Journal of Geophysical Research*, *109*, A12301. https://doi.org/10.1029/2004JA010583

Chau, J. L., & Woodman, R. F. (2001). Interferometric and dual beam observations of daytime spread-*F*-like irregularities over Jicamarca. *Geophysical Research Letters*, *28*(18), 3581–3584. https://doi.org/10.1029/2001GL013404

Fejer, B. G., de Paula, E. R., González, S. A., & Woodman, R. F. (1991). Average vertical and zonal F region plasma drifts over Jicamarca. *Journal of Geophysical Research*, *96*(A8), 13,901–13,906. https://doi.org/10.1029/91JA01171

Hanson, W. B., & Moffett, R. J. (1966). Ionization transport effects in the equatorial *F* region. *Journal of Geophysical Research*, *71*(23), 5559–5572. https://doi.org/10.1029/JZ071i023p0559

Hanson, W. B., & Sanatani, S. (1973). Large Ni gradients below the equatorial *F* peak. *Journal of Geophysical Research*, *78*(7), 1167–1173. https://doi.org/10.1029/JA078i007p01167

Heelis, R. A., Stoneback, R., Earle, G. D., Haaser, R. A., & Abdu, M. A. (2010). Medium scale equatorial plasma irregularities observed by Coupled Ion-Neutral Dynamics Investigation sensors aboard the Communication Navigation Outage Forecast System in a prolonged solar minimum. *Journal of Geophysical Research*, *115*, A10321. https://doi.org/10.1029/2010JA015596

Huang, C.-S., de La Beaujardiere, O., Roddy, P. A., Hunton, D. E., Ballenthin, J. O., & Hairston, M. R. (2013). Long-lasting daytime equatorial plasma bubbles observed by the C/NOFS satellite. *Journal of Geophysical Research: Space Physics*, *118*, 2398–2408. https://doi.org/10.1002/jgra.50252

Hysell, D. L., Larsen, M. F., Swenson, C. M., Barjatya, A., Wheeler, T. F., Sarango, M. F., et al. (2005). Onset conditions for equatorial spread *F* determined during EQUIS II. *Geophysical Research Letters*, *32*, L24104. https://doi.org/10.1029/2005GL024743

Immel, T. J., Mende, S. B., Frey, H. U., Peticolas, L. M., & Sagawa, E. (2003). Determination of low latitude plasma drift speeds from FUV images. *Geophysical Research Letters*, *30*(18), 1945. https://doi.org/10.1029/2003GL017573

Kil, H., Demajistre, R., & Paxton, L. J. (2004). *F*-region plasma distribution seen from TIMED/GUVI and its relation to the equatorial spread *F* activity. *Journal of Geophysical Research*, *31*, L05810. https://doi.org/10.1029/2003GL018703

Kil, H., & Heelis, R. A. (1998). Global distribution of density irregularities in the equatorial ionosphere. *Journal of Geophysical Research*, *103*(A1), 407–417. https://doi.org/10.1029/97JA02698

Kil, H., Paxton, L. J., & Oh, S.-J. (2009). Global bubble distribution seen from ROCSAT-1 and its association with the pre-reversal enhancement. *Journal of Geophysical Research*, *114*, A06307. https://doi.org/10.1029/2008JA013672

Kudeki, E., & Bhattacharyya, S. (1999). Postsunset vortex in equatorial *F*-region plasma drifts and implications for bottomside spread *F*. *Journal of Geophysical Research*, *104*(A12), 28,163–28,170. https://doi.org/10.1029/1998JA900111

Makela, J. J., & Kelley, M. C. (2003). Field-aligned 777.4-nm composite airglow images of equatorial plasma depletions. *Geophysical Research Letters*, *30*(8), 1442. https://doi.org/10.1029/2003GL017106

Martinis, C., Eccles, J. V., Baumgardner, J., Manzano, J., & Mendillo, M. (2003). Latitude dependence of zonal plasma drifts obtained from dual-site airglow observations. *Journal of Geophysical Research*, *108*(A3), 1129. https://doi.org/10.1029/2002JA009462

Mendillo, M., & Baumgardner, J. (1982). Airglow characteristics of equatorial plasma depletions. *Journal of Geophysical Research*, *87*(A9), 7641–7652. https://doi.org/10.1029/JA087iA09p07641

Narayanan, V. L., Sau, S., Gurubaran, S., Shiokawa, K., Balan, N., & Emperumal, K. (2014). A statistical study of satellite traces and subsequent evolution of equatorial spread *F* based on ionosonde observations over dip equatorial site Tirunelveli, India. *Earth, Planets and Space*, *66*(1), 160. https://doi.org/10.1186/s40623-014-0160-4

Pimenta, A. A., Bittencourt, J. A., Fagundes, P. R., Sahai, Y., Buriti, R. A., Takahashi, H., & Taylor, M. J. (2003). Ionospheric plasma bubble zonal drifts over the tropical region: A study using OI 630 nm emission all-sky images. *Journal of Atmospheric and Solar-Terrestrial Physics*, *65*(10), 1117–1126. https://doi.org/10.1016/S1364-6826(03)00149-4

Shiokawa, K., Otsuka, Y., Ogawa, T., & Wilkinson, P. (2004). Time evolution of high-altitude plasma bubbles imaged at geomagnetic conjugate points. *Annales Geophysicae*, *22*(9), 3137–3143. https:/doi.org/1432-0576/ag/2004-22-3137, https://doi.org/10.5194/angeo-22-3137-2004

Smith, J. M., & Heelis, R. A. (2018). The plasma environment associated with equatorial ionospheric irregularities. *Journal of Geophysical Research: Space Physics*, *123*, 1583–1592. https://doi.org/10.1002/2017JA024933

Su, S.-Y., Liu, C. H., Ho, H. H., & Chao, C. K. (2006). Distribution characteristics of topside ionospheric density irregularities: Equatorial versus midlatitude regions. *Journal of Geophysical Research*, *111*, A06305. https://doi.org/10.1029/2005JA011330

Tsunoda, R. T. (1983). On the generation and growth of equatorial backscatter plumes: 2. Structuring of the west walls of upwellings. *Geophysical Research Letters*, *88*(A6), 4869–4874. https://doi.org/10.1029/10.1029/JA088iA06p04869

Tsunoda, R. T., Livingston, R. C., & Rino, C. L. (1981). Evidence of a velocity shear in bulk plasma motion associated with the post-sunset rise of the equatorial *F*-layer. *Geophysical Research Letters*, *8*(7), 807–810. https://doi.org/10.1029/GL008i007p00807

Woodman, R. F., & La Hoz, C. (1976). Radar observations of *F*-region equatorial irregularities. *Journal of Geophysical Research*, *81*(31), 5447–5466. https://doi.org/10.1029/JA081i031p05447

Woodman, R. F., Pingree, J. E., & Swartz, W. E. (1985). Spread-*F*-like irregularities observed by the Jicamarca radar during the daytime. *Journal of Atmospheric and Solar-Terrestrial Physics*, *47*(8-10), 867–874. https://doi.org/10.1016/0021-9169(85)90061-3

Yokoyama, T., Yamamoto, M., Otsuka, Y., Nishioka, M., Tsugawa, T., Watanabe, S., & Pfaff, R. F. (2011). On postmidnight low-latitude ionospheric irregularities during solar minimum: 1. Equatorial Atmosphere Radar and GPS-TEC observations in Indonesia. *Journal of Geophysical Research*, *116*, A11325. https://doi.org/10.1029/2011JA016797